A Comparison of Different Techniques for Induction Motor Rotor Fault Diagnosis

A Alwodai, F Gu and A D Ball
Centre for Diagnostic Engineering, University of Huddersfield, Queensgate, Huddersfield HD1 3DH, UK

E-mail: a.alwodai@hud.ac.uk

Abstract. The problem of failures in induction motors is a large concern due to its significant influence over industrial production. Therefore a large number of detection techniques were presented to avoid this problem. This paper presents the comparison results of induction motor rotor fault detection using three methods: motor current signature analysis (MCSA), surface vibration (SV), and instantaneous angular speed (IAS). These three measurements were performed under different loads with three rotor conditions: baseline, one rotor bar broken and two rotor bar broken. The faults can be detected and diagnosed based on the amplitude difference of the characteristic frequency components of power spectrum. However IAS may be the best technique because it gives the clearest spectrum representation in which the largest amplitude change is observed due to the faults.

Keywords: Induction motor, Broken bar, Motor current signature analysis, Vibration, Instantaneous angular speed (IAS), Power spectrum.

1. Introduction

Three-phase induction motors are industry's workhorses and widely used as electromechanical energy conversion devices. Although induction machines are considered relatively reliable and robust due to their simple design and well-developed manufacturing technologies, failures do occur and may severely disrupt industrial processes and even lead to disastrous accidents. To prevent these failure happen, many techniques have been developed for early condition monitoring. Amongst the different methods, three of them are mostly studied because of their good performance of fault diagnosis for many machines.

The first one is the motor current signature analysis (MCSA). As a non-invasive monitoring technique it is sensitive to many motor faults such as broken bar and bearing damages. In addition it is convenient to be implemented in many applications. For these reasons, a large amount of research has been directed toward the analysis of motor current [1-5]. The second one is the surface vibration analysis. It is the main stream monitoring technique used widely in detecting motor bearing and broken rotor bar faults [7, 8]. Finally, IAS technique has been investigated recently by many researchers for condition monitoring and obtained very promising results [9, 10].

A comparison of stator current, vibration, and acoustic methods in detecting broken bar and bearing faults were presented by [11]. The detection and diagnosis of induction motor bearing faults were performed using vibration monitoring, acoustic emission and shock pulse along with stator current harmonics measurements [12]. They provide a very useful basis for determining an optimal technique or several redundant techniques for implementation of condition monitoring. To benchmark the newly

developed IAS with other two more conventional methods, this paper focuses on making a comparison of these three methods in detecting rotor bar faults, which takes account for up to 10% of overall motor faults.

Signal processing is essential for any techniques to obtain reliable and accurate motoring results. Processing methods range from time domain statistical analysis to joint time–frequency analysis, and include the uses of artificial neural network and wavelet transforms [9]. Spectral analysis of motor current signatures was performed by [10]. Wavelet packet decomposition (WPD) method was applied to analyze the characteristics of the stator current under normal and faulty conditions by [13]. The characteristics extracted from the WPD were then used detect rotor bar breakage and air-gap eccentricity faults. Rather than using very complicated methods, this comparison just applies conventional Fourier analysis approaches to obtain power spectra of each measurement so that the comparison is made on the same base that can be implemented realistically in condition monitoring.

The paper is organised into 7 sections. Following this introduction, the basic principles of the three techniques in monitoring the broken bars are outlined respectively in section 2, 3, and 4. Section 5 presents the details of measurement systems and faults induced. Section 6 presents the comparison results. Finally the conclusion obtained in this comparison is presented in section 7.

2. Motor Current Signature Analysis

Over the past few decades, condition monitoring techniques of induction motors have been extensively conducted with an emphasis on motor current signature analysis (MCSA). MCSA is a significant technique that uses for detecting faults of the induction machine, such as turn to turn fault in the stator, broken rotor bar and air-gap eccentricity [2-5]. Because of its strong advantages in machine diagnosis, this technique is often chosen as a fault analysis method for additional investigation.

Motor current signature analysis is based on detection of current harmonics with frequencies that are distinguishing each category of fault. In additional, it does not need additional installation of measurement system.

Broken bars cause the rotor asymmetry, the distortion of the rotor current distribution and therefore the changes in rotor magnetomotive force (MMF). A broken rotor bar fault has distinctive characteristic frequencies which can be calculated as

$$f_{brb} = f_s(1 \pm 2ks) \qquad k = 1, 2, 3 \ldots\ldots \tag{1}$$

The per unit slip of the motor can be calculated as

$$s = \frac{f_{slip}}{f_{sync}} = \frac{2f_s/p - f_r}{2f_s/p} \tag{2}$$

Where f_s and f_r are supply frequency and motor frequency respectively, and p is number of poles.

In case of broken bar, sidebands around the supply frequency can be expected in the phase current power spectrum. As a result, the first-order sidebands (k=1) are of particular significance in the detection of broken rotor bar fault. The left sideband $f_s(1 - 2ks)$ is due to electrical or magnetic rotor asymmetry caused by broken rotor bars while the right sideband $f_s(1 + 2ks)$ is due to the speed ripple or variation [6]. The amplitudes and presence of the sidebands depend on the physical position of the broken rotor bars, speed and load. The locations of the sidebands will shift outwards as the speed and load are increased. It is recognized that the sidebands might be observed when the motor has no broken rotor bar fault as rotor ellipticity and shaft misalignment could both induce rotor asymmetry to a certain extent [14]. However, the sideband amplitudes formed in those cases are much smaller compared with those produced by broken rotor bar fault. In this paper, two faulty motors were used, one with one broken rotor bar and the other motor with two broken bars. The rotors of these motors were drilled and used in the tests to simulate the broken rotor bar fault and then compared with a healthy motor.

Figure 1 and figure 2 show the two tested rotors with one broken bar and two broken bars respectively. Faults were induced by drilling carefully into the bars along their height in such a way that the hole cut the bar completely.

Figure 1. Rotor with one bar breakage.

Figure 2. Rotor with two bar breakage.

3. Motor Vibration Analysis

Accurate speed and mains frequency as well as fault related frequencies can be determined by using motor vibration spectrum. There are always inherent rotor mass unbalance and shaft misalignment leading to frequency components at motor rotation frequency f_r and its harmonics in vibration spectrum. As mentioned in section 2, in the case of broken rotor bar, there is a speed oscillation with frequency $2sf_s$.This oscillation acts as a frequency modulation on rotation frequency and two side band frequencies $f_r - 2sf_r$ and $f_r + 2sf_r$ appear around f_r in vibration spectrum [15]. When the rotor circuit unbalance increases, the magnitude of speed oscillation as well as the magnitudes of side band frequencies increase too. Therefore, the magnitudes of $f_r \pm 2sf_r$ can be good measures for broken bar detection. This paper has presented this method to detect broken bar faults by using vibration.

4. Instantaneous Angular Speed

A large number of techniques can be used to extract IAS from an encoder shaft signal. These techniques including carrier tracking, pulse timing, frequency domain block-shift transforms, frequency domain zoom demodulation and Hilbert transforms [16]. The accuracy of the first two techniques: (carrier tracking and pulse timing) is determined by the hardware resources available. This limits the wide application due to the cost of the required hardware and the non-generic nature of these techniques. The last three techniques use essentially the same principles to obtain the IAS signals. These methods are developed based on fast Fourier transform (FFT). This paper focuses extracting IAS based on Hilbert transform.

4.1. Analytic representation of measured IAS data

The IAS data is a pulse train modulated in phase by rotational oscillation. To get the oscillation or IAS, this study uses a Hilbert demodulation based method, which gives more accurate demodulation for the IAS. Supposing the pulse train signal is denoted by signal $s(t)$, its analytic form $z(t)$ can be constructed a real signal $s_r(t)$ and an imaginary part $s_i(t)$.

$$z(t) = s_r(t) + j\, s_i(t) \; = A(t)e^{j\beta(t)} \tag{3}$$

The amplitude A(t) and phase β(t) of the signal can be defined as [17]

$$A(t) = \sqrt{s_r^2(t) + s_i^2(t)} \tag{4}$$

$$\beta(t) = tan^{-1} \frac{s_i(t)}{s_r(t)} \tag{5}$$

The instantaneous frequency can be defined as the differentiation of the instantaneous phase with respective to time [17, 18]:

$$\omega(t) = \frac{d\beta(t)}{dt} \tag{6}$$

The question is how to define the imaginary part $s_r(t)$ of a complex signal $z(t)$ so that the instantaneous phase was correctly computed. If $s(t)$ is a real valued signal with spectrum $S(\omega)$ which can be given as [17]

$$S(\omega) = \frac{1}{2\pi} \int_{-\infty}^{\infty} s(t) e^{-j\omega t} dt \tag{7}$$

The complex signal called analytical signal $z(t)$ is obtained from $S(\omega)$ by inverse Fourier transform, where the integration runs only over positive frequencies [18]

$$z(t) = 2 \frac{1}{\sqrt{2\pi}} \int_{0}^{\infty} S(\omega) e^{-j\omega t} d\omega \tag{8}$$

Resulting relation describing analytical signal $z(t)$ [18]

$$z(t) = s(t) + \frac{j}{\pi} \int_{-\infty}^{\infty} \frac{s(\tau)}{t-\tau} d\tau \tag{9}$$

The imaginary part of equation (9) is called Hilbert transformer of $s(t)$

4.2. The demodulation using Hilbert transformation

The direct definition of Hilbert transform was introduced in section 4.1. This definition is not suitable for the transform computation. In reality, the FFT is used for the transform computation. The spectrum of a measured real signal is multiplied by $-j$ (vector rotation by $-\pi/2$) and then the Inverse Fourier Transform is used. The result is the complex part of the analytical signal [17].

The angle $\beta(t)$ represents the phase of the analytical signal and is computed according to equation (5). Phase determination $\beta(t)$ from a complex number position holds only in the range $\langle -\pi, \pi \rangle$ and if the phase overlaps this region, it is necessary to unwrap it and moreover to remove the phase trend component which moves up by 2π every revolution with the increase of the common phase carrier signal.

The phase unwrapping corrects the radian phase angles by adding multiples of $\pm 2\pi$ when absolute jumps between consecutive elements of $\beta(t)$ are greater than the default jump tolerance of π radians. If the jump is lower than $-\pi$, 2π radians are added, if the jump is greater than π, 2π is subtracted. The result is an unwrapped phase. Removing the trend means the subtraction of a partial part of the overall angle from every sample of the unwrapped phase. It really represents the angle time course tilting to the time axis.

For IAS based diagnosis, the characteristic frequency can be identified in the low frequency range of its power spectrum. The broken bar causes directly an oscillation torque, which induces a fluctuation of rotor speed. According to the analysis made in [19], the oscillation of rotor is at *2sf* and has been observed in IAS spectrum in [20]. Therefore, the frequency peak can be located at the slip pole frequency f_{sp}. Following previous symbols, it can be calculate by

$$f_{sp} = p\, f_{slip} = p\, s \frac{2f_s}{p} = 2sf_s \tag{10}$$

One can see from equation (10) the slip pole frequency is not dependent on the number of motor poles.

5. Experimental Methods

Figure 3 shows schematic diagram of the induction motor test facility. The system consists of an induction motor, variable speed controller, supporting bearings, couplings and DC generator as a load. The test motor is a three-phase induction motor with rated output power of 4 kW at speed 1420rpm (two-pole pairs). To change the speed of the motor, a digital variable speed controller is attached to the test rig between the power line source and the motor. The controller can be programmed to any specific shaft rotation speed between 0 and 3600 RPM. The induction motor is directly coupled with a loading DC generator. The field of the generator is connected to DC source through controller while the generated power was fed back to the mains electrical grid and the load in the induction motor can be adjusted by changing the field resistance of the DC generator. The operating load can be varied from no load to full load via the control panel.

A power supply measurement box was designed to measure AC voltages, currents and power, using Hall Effect voltage and current transducers and a universal power cell. A piezoelectric accelerometer, mounted on the bearing end-caps, is used to measure vibration of the motor. It has a sensitivity 5.106 mV/ms2 frequency range: 0.5 to 5000Hz. A shaft encoder, mounted on the shaft end as shown in Figure 4, produces 100 pulses per revolution for measuring the IAS signals. According to [21], the basic resolution of this measurement system is 2.47%.

During the experimental work all the data was acquired using a GST YE6232B data acquisition system. This system has 16 channels, each channel with a 24 bit analogue-digital converter with a maximum sampling frequency of 96 kHz. Tests were carried out for four different loads with the healthy motor, one broken bar motor and two broken bars motor.

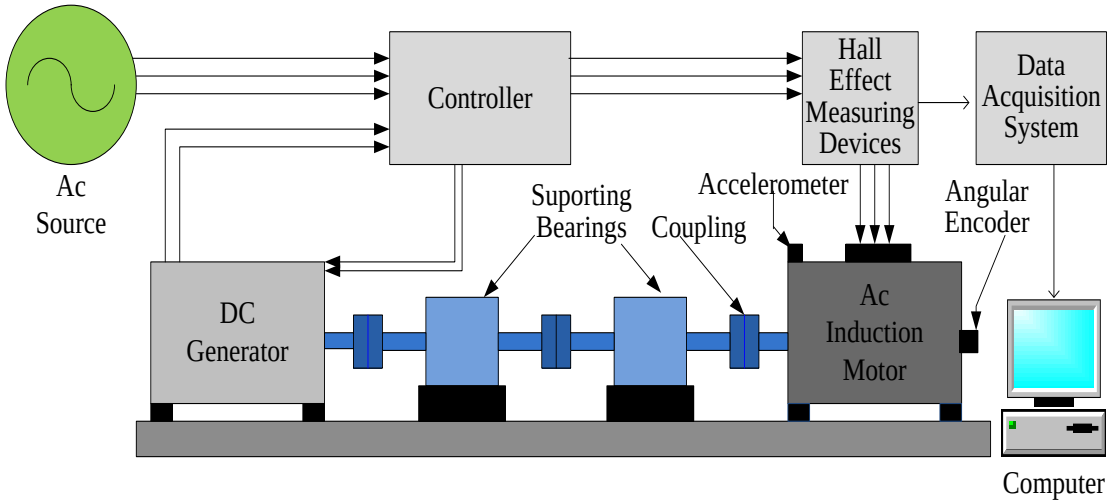

Figure 3. Schematic diagram of the induction motor test facility.

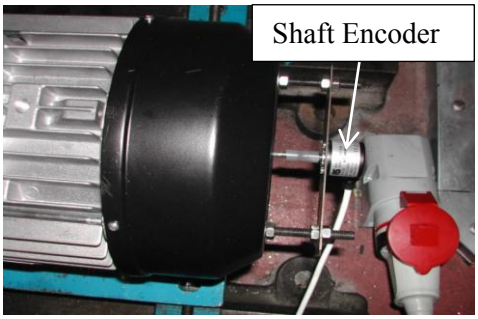

Figure 4. Hengstler shaft encoder.

6. Results and Discussions

MCSA, Vibration and IAS data sets are processed to obtain their power spectra with a same windows size so that the characteristic frequency can be identified for comparison under different load conditions.

6.1. Broken bar fault detection by MCSA

Figure 5 shows the current power under healthy and faulty motor at different loads. The sideband amplitudes of healthy motor are -27.27 dB (left) and -34.38 dB (right), while they are -16.19 dB (left) and -19.03 dB (right), and -13.01dB (left) and -14.80 dB (right) in case of two broken bars, The difference amplitude of left sidebands between healthy and two broken bars is 14.26 dB at 75% full load. It is clear that the amplitude of side band increase as the load and fault severity increase and that the fault can be best detected under higher loads.

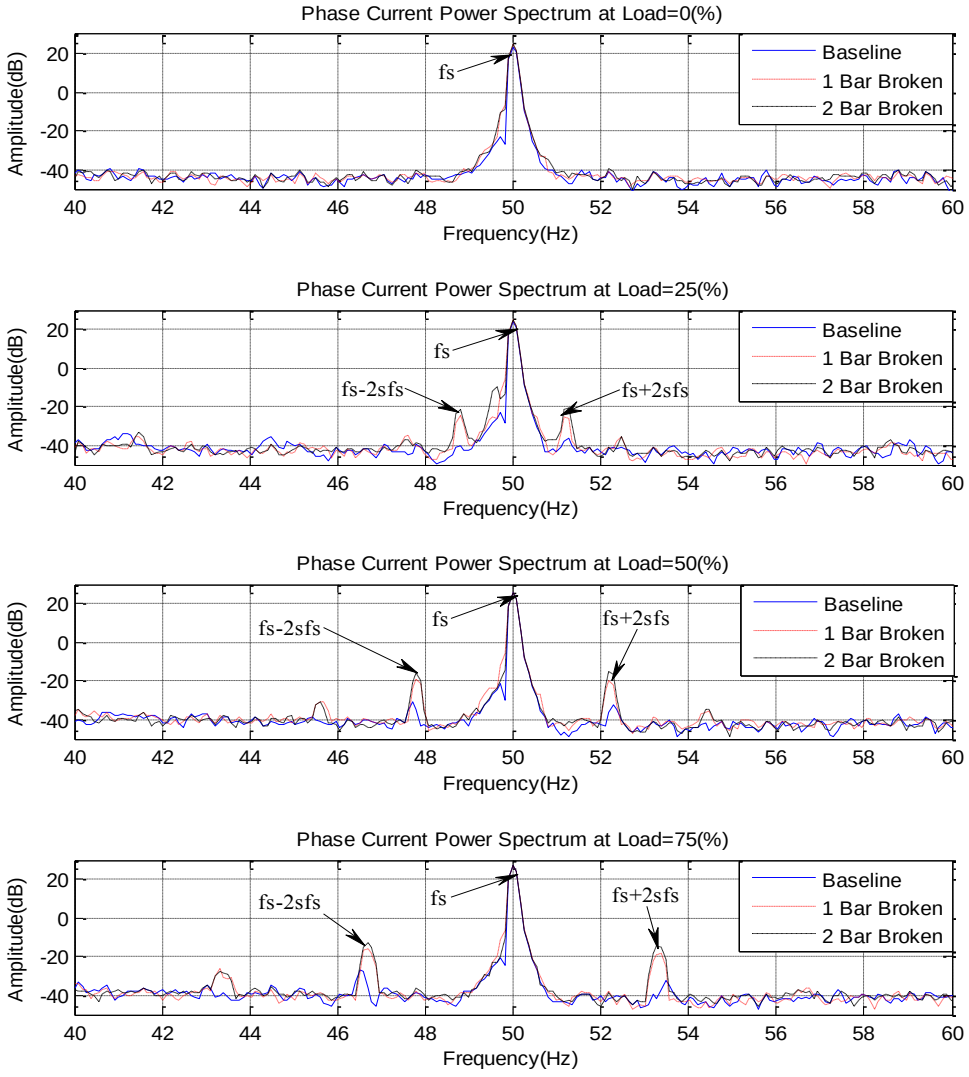

Figure 5. Phase current power spectra under different load conditions.

Table 1. Comparison results of motor current.

Load	Sideband(dB) of healthy motor		Sideband amplitude (dB) of one broken bar				Sideband amplitude (dB) of two broken bars			
	L	R	L	Δ_{1L}	R	Δ_{1R}	L	Δ_{2L}	R	Δ_{2R}
25%	-38.12	-35.62	-25.61	+12.51	-21.15	+14.47	-21.51	+16.61	-21.15	+14.47
50%	-31.30	-34.50	-20.29	+11.01	-20.51	+13.99	-16.20	+15.10	-16.04	+18.46
75%	-27.27	-34.38	-16.19	+11.08	-19.03	+15.35	-13.01	+14.26	-14.80	+19.58

L : the left sideband ; R : the right sideband; Δ_{1L}, Δ_{1R} : the deference between left and right sidebands of healthy and one broken bar ; Δ_{2L}, Δ_{2R} : the deference between left and right sidebands of healthy and two broken bar

Table 1 shows MCSA power spectrum comparisons of both the left and right sideband amplitudes between a normal and broken rotor bar at four load conditions, namely 0%, 25%, 50% and 75% full load.

6.2. Broken bar fault detection by motor vibration

Figure 6 show the power spectrum motor vibration under different load. As can be seen from the figure, sideband differences between normal and broken rotor bar on both sides of the rotor speed f_r at 75% full load. Under the normal condition, amplitudes of the first-order sidebands are around -59.47 dB (left) and -55.18 dB (right), respectively. With one broken bar fault the sideband amplitudes are increased to -57.81dB and -54.52 dB, a difference of 4.29 dB, while sidebands are -53.35 and -49.05 dB in case of two broken bars. Table 2 provides a full comparison at both the left and right sideband between three cases under four load conditions, namely 0%, 25%, 50% and 75% full load. In general the amplitude difference becomes larger as load and fault severity increase.

It is also observed from Figure 6 that the frequency of the maximum amplitude shifts leftward as the load increases. This is because this frequency links to the speed of the rotor, which is slower than the speed of the magnetic fields (25 Hz) due to the load effect of slip.

Table 2. Comparison result of motor vibration.

Load	Sideband(dB) of healthy motor		sideband amplitude (dB) of one broken bar				sideband amplitude (dB) of Two broken bars			
	L	R	L	Δ_{1L}	R	Δ_{1R}	L	Δ_{2L}	R	Δ_{2R}
25%	-61.52	-67.72	-60.17	+1.35	-59.25	+8.47	-57.49	+4.03	-58.79	+8.93
50%	-66.6	-62.86	-59.03	+7.57	-57.63	+5.23	-53.78	+12.82	-51.42	+11.44
75%	-59.47	-55.18	-57.81	+1.66	-54.52	+0.66	-53.35	+6.12	-49.05	+6.13

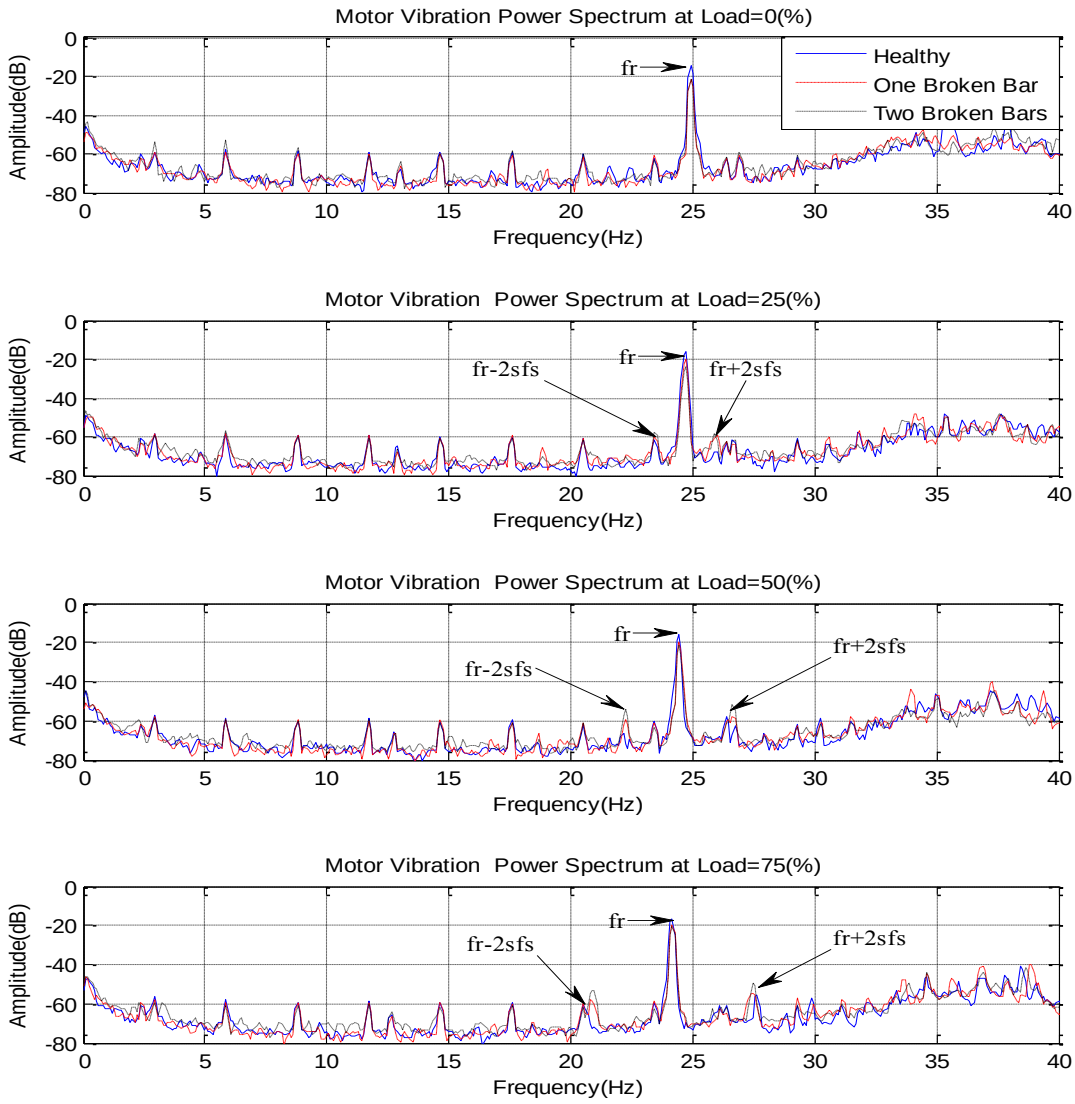

Figure 6. Motor vibration power spectra under different load conditions.

6.3. Broken bar fault detection by IAS

Figure 7 shows the power spectra of IAS at different load and under normal and broken rotor bar condition. The evolution of the modulation amplitudes is clearly visible from the magnitudes of spectral peaks at corresponding frequency ($slip\ pole\ frequency = 2sf_s$) which increases as the load increases.

Under no-load condition the amplitudes of IAS at slip pole frequency (0.55 Hz) are -19.54 dB, -16 dB and -12.76 dB under healthy, one broken and two broken bars condition respectively. With 25% full load the IAS amplitudes at related slip pole frequency (1.19 Hz) are -23.68 dB, -5 dB and -1.38 dB under three motor operation conditions. In case of 50% load IAS amplitudes are -14.21 dB, -0.1 dB and 4.27 dB at frequency (2.3 Hz) and under healthy one broken bar and two broken bars. The last case is with 75% load, IAS amplitudes are -10.8 dB, 1.645 dB and 6.52 dB at frequency (3.3 Hz) and under healthy one broken bar and two broken bars.

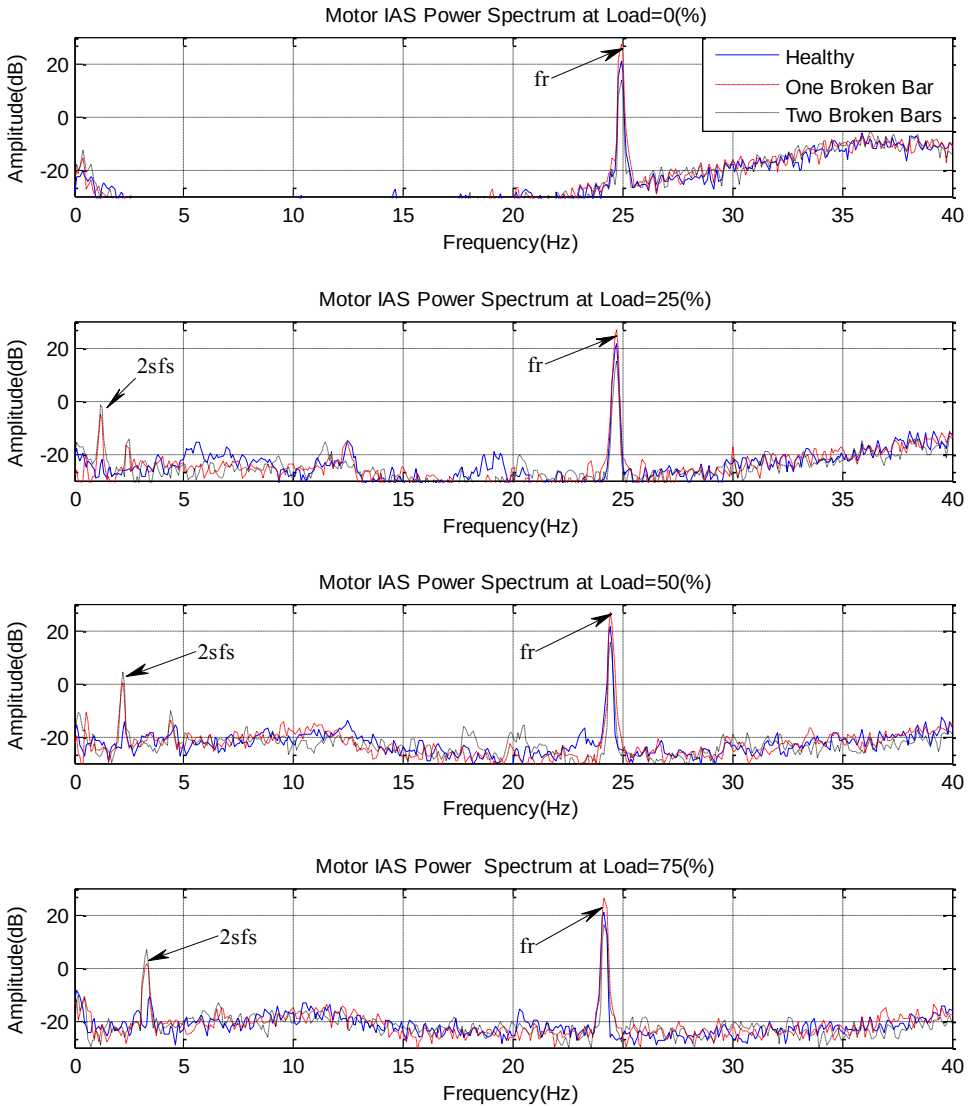

Figure 7. IAS power spectra under different load conditions.

6.4. Comparison between techniques

The comparative study of different condition monitoring techniques has been done for healthy motor and broken bar condition. It is noted that sideband amplitudes of broken rotor bar are higher than the corresponding normal sideband amplitudes. The difference between sideband amplitudes of healthy and two broken bar is 14.23 dB at 75% load with MCSA while it is only 6.12 dB with motor vibration method. Interestingly, IAS power spectrum amplitude has a 17.32 dB change. Consequently, IAS performs best in detecting the rotor bar faults.

In addition, IAS spectrum is also the simplest one, showing clearly the fault frequency components.

7. Conclusions

Motor current, surface vibration and instantaneous angular speed are evaluated experimentally to monitor broken rotors. From their spectrum presentations, it has been shown that they all allow a full diagnosis of the rotor bar faults under high load conditions.

The spectrum of stator current signatures shows that the amplitude of sidebands around the supply frequency increases with fault severity increases. In a similar way, the sidebands of surface vibration also increase in amplitudes with load but they appear at rotor frequency. Interestingly, IAS has no modulation influences and its spectrum shows the faults at a low frequency range which is much clearer that makes it easy to identify and quantify the characteristic frequency of different bar breakages.

References

[1] Thomson W T. and Fenger M 2001 Current signature analysis to detect induction motor faults *IEEE Industry Applications Magazine* pp 26–34

[2] Alwodai A, Gu F and Ball A 2011 Motor Current Signature Analysis of a Variable Speed Drive for Motor Fault Diagnosis Proceedings of the 24th COMADEM2011 (Stavanger: Norway) pp 884–892

[3] Stavrou A, Sedding H G and Penman J 2001 Current Monitoring for Detecting Inter-turn Short Circuits in Induction Motors IEEE Transactions on Energy Conversion **16** pp 32–37

[4] Benbouzid MA 2000 A Review of Induction Motors Signature Analysis as a Medium for Faults Detection *IEEE transactions on industrial electronics* **14** pp 984–93

[5] Mehla N Dahiya R 2007 An Approach of Condition Monitoring of Induction Motor Using MCSA *International Journal of Systems Applications Engineering & Development* **1** pp 13–17

[6] Filippetti F, Franceschini G, Tassoni C and Vas P 1998 AI techniques in induction machines diagnosis including the speed ripple effect *IEEE Transactions on Industry Applications* **34** pp 98–108

[7] Betta G, Paolillo A., and Pietrosanto A 2002 A DSP-based FFT analyzer for the fault diagnosis of rotating machine based on vibration analysis *IEEE Transactions on Instrumentation and Measurement* **51** pp 1316–22

[8] Ocak H and Loparo K A., 2004 Estimation of the running speed and bearing defect frequencies of an induction motor from vibration data *Mechanical Systems and Signal Processing* **18** pp 515–533

[9] Benbouzid M and Kliman G 2003What stator current processing-based technique to use for induction motor rotor faults diagnosis? *IEEE Transactions on Energy Conversion* **18** pp 238–244

[10] Benbouzid M, Nejjari H, Beguenane, R and Vieira M 1999 Induction motor asymmetrical faults detection using advanced signal processing *techniques IEEE Transactions on Energy Conversion* **14** pp147–52

[11] LI W and Mechefske C 2006 Detection of Induction Motor Faults: A Comparison of Stator Current, Vibration and Acoustic Methods *Journal of Vibration and Control* **12** pp 165–88

[12] Tandon N, Yadava G and Ramakrishna K 2005 A comparison of some condition monitoring techniques for the detection of defect in induction motor ball bearings *ITMME Centre Indian Institute of Technology* (New Delhi India) pp 244–256

[13] Ye Z, Wu B and Sadeghian A 2003 Current signature analysis of induction motor mechanical faults by wavelet packet decomposition *IEEE Transactions on Industrial Electronics* **50** pp 1217–28

[14] Yazlcl B and Kliman G 1999 An adaptive statistical time–frequency method for detection of broken bars and bearing faults in motors using stator current *IEEE Transactions on Industry Applications* **35** pp 442–52

[15] Sadoughi A, Ebrahimi M and Rezaei E 2006 A new approach for induction motor broken bar diagnosis by using vibration spectrum *SICE-ICASE International Joint Conference* Bexco Busan Korea pp 4715–20

[16] Sweeney P and Randall, R 1996 Gear transmission error measurement using phase demodulation *Proc. Instn. Mech. Engineers* **210** pp 201–213

[17] Ben Sasi A Y, Gu F, Payne B and Ball A 2004 Instantaneous angular speed monitoring of electric motors *Journal of Quality in Maintenance Engineering* **10** pp 123–135
[18] Shi D, Unsworth P J, and Gao R X 2006 Sensorless Speed Measurement of Induction Motor Using Hilbert Transform and Interpolated Fast Fourier Transform *IEEE Transactions on Instrumentation and Measurement* **55** pp 290–299
[19] Bellini A, Filippetti F, Franceschini G, Tassoni C and Kliman G B 2001 Quantitative evaluation of induction motor broken bars by means of electrical signature analysis *IEEE Transactions on Industry Applications* **37** pp 1248-55
[20] Ben Sasi A Y, Gu F, Li Y and Ball A D 2006 A validated model for the prediction of rotor bar failure in squirrel-cage motors using instantaneous angular speed *Mechanical Systems and Signal Processing* **20** pp 1572–89
[21] Li Y, Gu F, Harris G, Ball A, Bennett N and Travis K 2005 The measurement of instantaneous angular speed *Mechanical Systems and Signal Processing* **19** pp 786–805